Research & Reviews: Journal of Material Sciences
DOI: 10.4172/2321-6212.S1-001

e-ISSN:2321-6212
p-ISSN:2347-2278

Characterization of Mo-AlNxOy Thin Films Deposited by RF Magnetron Sputtering

Thyago Santos Braga[1*], Marcos Massi[2], Argemiro Soares Silva Sobrinho[1], Fabio Dondeo Origo[3], Choyu Otani[1]

[1]Technological Institute of Aeronautics, Plasmas & Processes Laboratory, 12228-900, São José dos Campos, SP, Brazil

[2]Technological Institute of Aeronautics, Plasmas & Processes Laboratory, 12228-900, São José dos Campos, SP, Brazil and Federal University of São Paulo, Institute of Science & Technology, 12231-280, São José dos Campos, SP, Brazil

[3]Institute for Advanced Studies, Laboratory of Optical Surface Measurements, 12228-001, São José dos Campos, SP, Brazil

Research Article

Received date: 17/10/2016
Accepted date: 26/10/2016
Published date: 05/11/2016

***For Correspondence**

Thyago Santos Braga, Technological Institute of Aeronautics, Plasmas & Processes Laboratory, 12228-900, São José dos Campos, SP, Brazil, Tel: +55 11 98235 5657

Email: thyago@ita.br

Keywords: Mo-AlNxOy; Magnetron sputtering; Thin films; Thermal annealing

ABSTRACT

Thin films of Mo-AlN_xO_y were grown on glass and silicon substrates by RF-reactive magnetron sputtering. The substrate deposition temperature was varied with the purpose of evaluating the composition variation, crystal structure, reflectance, absorptance and band gap of the films. The results showed that the most amorphous films presented the highest absorptance. The absorptance increase and the band gap reduction are due to the crystallinity and the molybdenum insertion. This change occurred due to the different behavior of band gap amorphous materials, the electron acceptors/donors increase and plasmon effect caused by molybdenum insertion.

INTRODUCTION

Nowadays, nitride compound semiconductors and nano-structured materials are widely used in optoelectronic and micro-electronics devices [1]. Among these materials, the oxynitrides (Metal-N_xO_y) have become promising candidates for various applications [2]. This new structure based on oxygen/nitrogen deposition promotes properties between insulating oxides (ionic metal–oxygen bonds) and metallic nitrides (covalent metal–nitrogen bond) [3], which provides a variation in band gap, morphological and electrical properties, promoting applications according to the particular application required [2]. Among these oxynitrides, AlN_xO_y, a semiconductor that has its properties tailored between aluminum oxide (Al_2O_3) and aluminum nitride (AlN), has become one of the most studied due its cubic polycrystalline and defect spinel structure which makes it possible to get transparent ceramics with high strength and good thermal stability, i.e., the property of the film to withstand high temperatures (~400ºC) without suffer any modification in this optical or morphological properties [4-6]. This material can be applied as protective coating against diffusion and corrosion [7,8], optical coating [9], metal insulator structures (MIS) [5], and may replace the conventional passivating films of Si_3N_4 or SiO_2 on p-silicon solar cells [5]. AlN_xO_y can be also used as biomaterial, i.e., UV radiation dosimetry, since AlN_xO_y possesses a spectral sensitivity similar to human skin [5,10]. Meanwhile, the available knowledge on this structure is still reduced and it is mainly related with its spinel structure and to the AlN and Al_2O_3 properties separately [11].

The main AlN characteristic that influences AlN_xO_y is its wurtzite structure. When stoichiometric it is a very stable compound with a strong covalent/ionic bonding (11.5 eV/bond) [12], and presents great technological advantage in several applications such as: surface acoustic wave (SAW), bulk acoustic wave (BAW), among being an attractive material due its high melting point (~2400ºC), thermal conductivity (260 to 320 $Wm^{-1}K^{-1}$), band gap (~6.2 eV), hardness (~$2.0x10^3$ $kgf.mm^{-2}$) and high electrical resistivity (ρ=109-1011 Ωm). In particular, AlN is also a promising candidate for optical applications, once it has high optical trans-

e-ISSN:2321-6212
p-ISSN:2347-2278

mission between 0.2-12.5 μm [12-16].

The other material, Al_2O_3, has some interesting properties such as high-k (k~10); hardness (Mohs 9), wide band gap (8~10 eV), conduction band offset (2.8 eV), and low leakage current (compared to SiO_2) [17-24]. In microelectronics, it is used as Dynamic Random Access Memories (DRAMs), Complementary-Metal-Oxide Semiconductors (CMOS), Metal Oxide Semiconductor Field Effect Transistor (MOSFETs), among others [19,21,22,24,25]. Furthermore, Al_2O_3 can be synthesized by several deposition methods such as sol–gel, electron-cyclotron-resonance sputtering and self-limiting atomic layer deposition [26].

A way of improving even more the semiconductors properties is the addition of a metallic phase with better electronic and thermal properties [27]. This kind of material with a ceramic matrix and metal-nanoparticles is known as cermet [28] and has been used in different applications such as solar energy conversion, optical wave-guides, photo-electrochemical and gas sensors [29]. In the present work, molybdenum was chosen due its low density when compared to other refractory metals (dth=10.2 g cm^{-3}) [30], corrosion resistance at high temperatures, melting point (2883 K), high thermal conductivity (138 $Wm^{-1}K^{-1}$), thermal expansion coefficient (~7.0x10^{-6} K^{-1} between 300 and 1200 K) close to AlN (~6.5x$10^{-6}K^{-1}$ for pure AlN in the same range of temperature) [27]. Furthermore, Mo addition (20 vol.%) in a AlN matrix improve its thermal conductivity from 78 $Wm^{-1}K^{-1}$ (pure AlN) to almost 104 $Wm^{-1}K^{-1}$. It was also shown that the bend strength and fracture toughness of Mo-AlN composites increased as a function of metal phase concentration. This improvement in the mechanical and thermal properties was attributed to the Mo ductile nature, higher mechanical resistance and adherent interface between the Mo grains and the AlN matrix.

In this paper, it was performed a morphological study of Mo-AlN_xO_y thin films grown on silicon substrates by magnetron sputtering technique.

MATERIAL AND METHOD

Mo-AlN_xO_y thin films were deposited on silicon wafers [p-Si (1 0 0), ρ ~8–12 ohm cm] [31] by radio frequency (RF) reactive sputtering using a 4.0 inch (100 mm) Al target (99.999%). The source of molybdenum was a rectangular metallic tape (101.6 mm x 2.0 mm x 4.2 mm - purity 99.9%) placed on the aluminum target. This dimension was chosen in order to produce a film with 5% of Mo in the film, i.e., after a series of deposition varying the width of the tape it was obtained a satisfactory reproducibility. Prior to Mo-AlN_xO_y film depositions, silicon wafers were cleaned by standard RCA cleaning process [31].

During the deposition, the applied power was 200 W and substrate temperature was varied between 473K (200ºC); 573K (300ºC) and 673K (400ºC), and the deposition time was 60 min. The sputtering vacuum chamber, made with a cylindrical shape with 24 cm length and 20 cm in diameter, was pumped down with a diffusion and mechanical pump to a base pressure lower than 9.3 × 10^{-4} Pa and the process pressure was 7,0 x 10^{-1} Pa. The films were prepared with the substrate positioned at 90 mm from the target.

The chemical composition of the films was investigated by Rutherford Backscattering Spectrometry (RBS) with scattering angle of 180º. Measurements were done at 2 MeV with He^{2+} and the data were analyzed with the RUMP v.4.00 (beta) software. The crystallinity of the films was evaluated by Phillips X-PERT-PRO X-Ray Diffraction (XRD) with Cu-Kα radiation (1.5406˚A) and grazing angle of 1.0º. Thickness where measured with an Alpha-Step 500 (Tencor) profilometer. Optical reflectance and transmittance was measured with a Jasco V570 UV-VIS-NIR spectrophotometer in the wavelength range of 0.2-2.0 μm using an integrating sphere coated with barium sulphate ($BaSO_4$). The solar absorptance (As) defined as the weighted average between the intensity of the absorbed radiation and the total radiation incident in a surface was calculated by Eq. 1 [32]:

$$A_s = \frac{\int_{\lambda_1}^{\lambda_2} (1 - R(\lambda)) I_s(\lambda) d\lambda}{\int_{\lambda_1}^{\lambda_2} I_s(\lambda) d\lambda} \quad (1)$$

The solar normal radiance (Is) used was AM 1.5, defined by the ISO standard 9845-1 (1992), R is the near normal hemispherical reflectance and λ the photon wavelength (λ_1= 0.3 μm and λ_2=2.5 μm) [32].

The optical band gap of the Mo-AlN_xO_y films was determined from transmittance and reflectance measurements obtained from the samples deposited on glass substrates. With these values it was possible to calculate the optical absorption coefficient (αA) that is directly related to the transmittance T and reflectance R, as shown by Eq. 2 [33]:

$$\alpha_A d = -ln\left(\frac{T}{1-R}\right) \quad (2)$$

where d is the thickness of the film. The energy band gap was calculated from the transmission spectra using Tauc's relation (Eq. 3) [34,35]:

$$\alpha_A h\upsilon = B\left(h\upsilon - E_g\right)^{r/2} \quad (3)$$

e-ISSN:2321-6212
p-ISSN:2347-2278

where B is a constant, hu is the photon energy of incident light, and Eg is the optical band gap. The optical band gap is obtained by extrapolating the tangential line to the photon energy axis in the plot of $(\alpha hu)^2$ as a function of hu [35], where r is a constant equal to 1.0 for direct band gap semiconducting, and 4.0 for an indirect band gap semiconducting [34,36]. In the present work r= 1.0, related to the AlN transition [35,36], so the Eq. 3 becomes:

$$\left(\alpha_A h\upsilon\right)^2 = B^2\left(h\upsilon - E_g\right) \quad (4)$$

RESULTS AND DISCUSSIONS

Chemical Composition

This section presents the results of the chemical composition via RBS of the Mo-AlN_xO_y films deposited at 200ºC, 300ºC and 400ºC. **Figure 1** shows the Mo-AlN_xO_y chemical composition suggesting that the stoichiometry of films deposited at 200ºC, 300ºC and 400ºC are Mo-Al1,0N1,001,0; Mo-Al1,0N1,001,5 and Mo-Al1,0N1,001,6, respectively. It can be observed the non-variation of the molybdenum concentration (≈5%), indicating that the tape attached to the target produced a film with a relatively homogeneous amount of Mo, and the film deposited at 200ºC presented an stoichiometric AlNO phase.

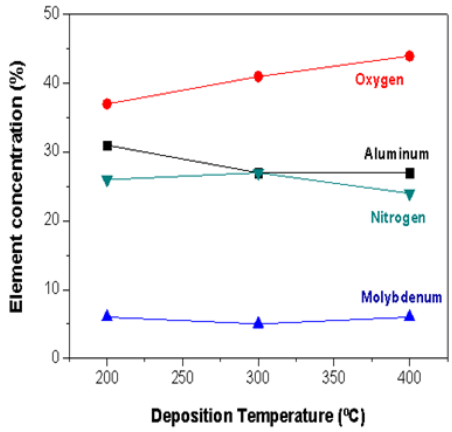

Figure 1. Chemical composition of the films deposited at 200, 300 and 400°C obtained from RBS.

The substrate temperature showed a modest influence in the nitrogen reaction during the deposition, however, the oxygen concentration was substantially influenced. The higher affinity and reactivity of oxygen with aluminum, when compared to the nitrogen, is explained by the Gibbs free energy values to aluminum oxide to formation (ΔG^0f, 298K (Al_2O_3)=-1.58x10^6 J.mol^{-1}) which is greater than aluminum nitride formation (ΔG^0f, 298K (AlN)=-2.87x10^5 J.mol^{-1}). Furthermore, the oxygen electronegativity is also higher than nitrogen (N2= 3.0 and O2= 3.5) which favors even more the aluminum reaction with oxygen [37-39].

X-ray Diffraction Studies of Mo-AlN_xO_y Films

Figure 2 shows the XRD spectra of the films deposited at 200ºC, 300ºC and 400ºC at 1.0º grazing angle. It can be observed three main peaks related to AlN (100) at 2θ ~33º [40,41]; AlON (400) at 2θ~53º, AlON (204) at 2θ ~72º [40-42] and molybdenum at 2θ ~40º [27].

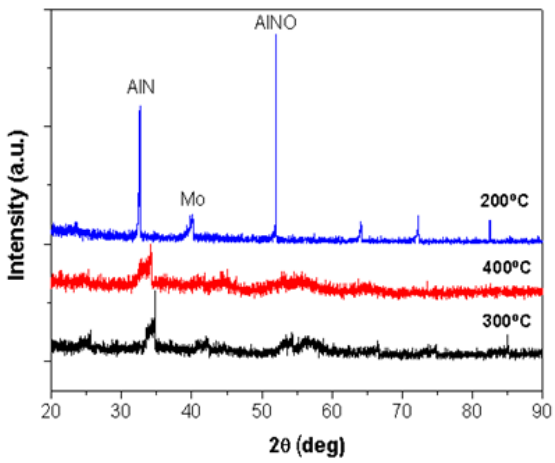

Figure 2. X-ray diffraction spectra for Mo-AlNxOy deposited at 200ºC; 300ºC; and 400ºC.

e-ISSN:2321-6212
p-ISSN:2347-2278

The spectra of the film deposited at 200ºC shows the highest crystallinity with a little displacement in the AlON and AlN peaks. However, the spectra of the film deposited at 300ºC and 400ºC show an almost amorphous structure with a broad AlN (100) peak at 2θ ~33º [40,41] in both films. This broad peak and angle (2θ) displacement may be due to the size variation of the AlN crystallites and microscopic deformation of the lattice due to insertion of molybdenum. Moreover, this result may also suggest that the film consists of tiny AlN crystallites embedded in an oxygen-rich amorphous matrix of Al_2O_3 [42-44]. These results may be related with the thin films study performed by Movchan and Demchishin [45,46]. In their study, it was described the microstructure of thin films trough structure-zone diagrams (SZD), taking into account the homologous temperature (Th), defined as the growth temperature of the film (T) normalized by the melting temperature of the deposited material (Tm) (Th= T/Tm). Since the temperature of the film is usually unknown, the substrate temperature is employed. Movchan and Demchishin [45,46] proposed three temperature zones related to homologous structures of the films: In the first zone (Th<0.3) thin films grown by evaporation exhibit a columnar structure and a porous contours of grain boundaries with a high density of defects in the crystal lattice; in the second zone temperature (0.3<Th<0.5) the films exhibit an amorphous or nanocrystalline structure; in the third zone, with high temperature counterpart (Th>0.5), crystalline grains are larger, and a denser film is obtained when compared to the intermediate zone (0.3<Th<0.5) [45-48]. This feature indicate that the present films of AlNxOy which melting temperature is 2165 °C (2438 K) [49], and substrate temperature 200 °C, 300 °C and 400 °C (673 K) leads to a homologous temperature Th ≈0.3. This value is the limit to entry into the second zone, which may generate a structure with characteristics such as: amorphous with imperfections in the crystal lattice and pores in its structure, which is correlated with the present film as shown by XRD.

These imperfections in the crystal lattice can be related to the deposition temperature which enhances the oxygen reaction due to the Gibbs free energy [1,37,50,51]. Brien, et al. [1], for example, observed that the AlN crystal structure not only depend on parameters such as power and deposition temperature, but is particularly related with the oxygen concentration in the film. In the present work, the film that showed the highest oxygen concentration showed the most amorphous structure (A400), and the film with the smallest amount of oxygen (A200) presented the most crystalline structure. It is noteworthy, that peaks related to Al_2O_3 phase were not observed in any films due to difficulty in obtaining crystalline phases of this material by magnetron sputtering process [8,52]. The growth of crystalline alumina (α-Al_2O_3) begins at ≈ 670 °C and for its complete crystallization temperatures above 700ºC are required [42,53].

Optical Analysis of Mo-AlN_xO_y

Figure 3 shows the reflectance of the films as deposition temperatures function. Considering that reducing the reflectance means an increase in absorptance [54], it can be highlighted that the film deposited at 400ºC showed the higher absorptance between 400 and 800 nm (visible and near infrared) when compared to the others.

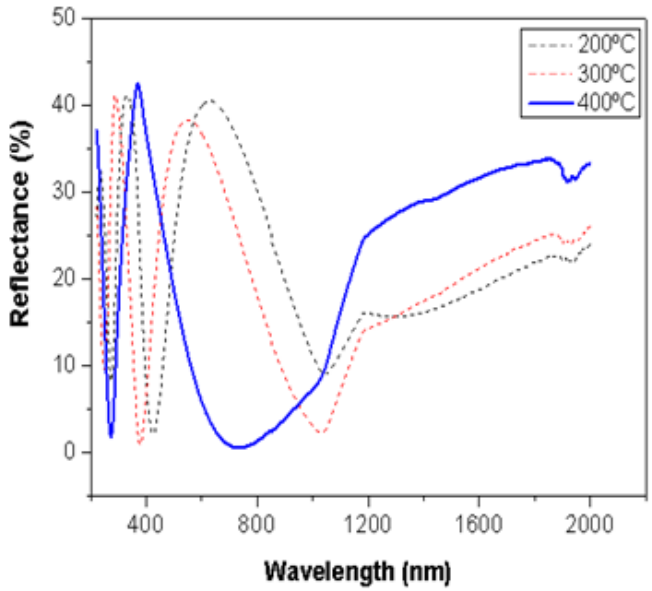

Figure 3. Mo-AlNxOy reflectance spectrum as function of the deposition temperature.

In **Figure 4** the solar absorptance (A_s) obtained by Eq. 1 increases gradually with the deposition temperature reaching the best value at 400ºC. However, the elemental composition analysis **(Figure 1)** shows that it was not the major factor influenced the solar absorptance.

One of the parameters that may have influenced the solar absorptance is the film thickness. The films deposited at 200, 300 and 400ºC presented thickness of 183, 169 and 109 nm, respectively. This thickness variation influences decisively the optical properties of this material. Ilican, et al. [55] studying the thickness and optical properties of zinc oxide (ZnO) concluded that the film thickness influences greatly its optical constants.

e-ISSN:2321-6212
p-ISSN:2347-2278

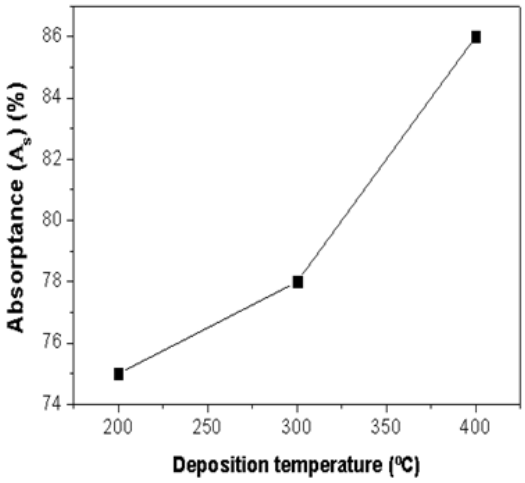

Figure 4. Solar absorptance (As) as function of the deposition temperature.

Another factor that may alter the film absorptance is the crystalline structure. The film deposited at 400ºC, which showed the highest absorptance, presented the most disorderly (amorphous) structure. O'Leary et al. [56] showed that an increase of the material structure disorder promotes a reduction of the empirical optical gap and broadening the absorption tail into the gap region, as can be seen in **Figure 5** [56]. This happens because in a defect-free crystalline semiconductor the optical absorption spectrum terminates abruptly at the energy gap. In contrast, in an amorphous semiconductor a tail in the absorption spectrum extends into the gap region, as can see in **Figure 5** [56].

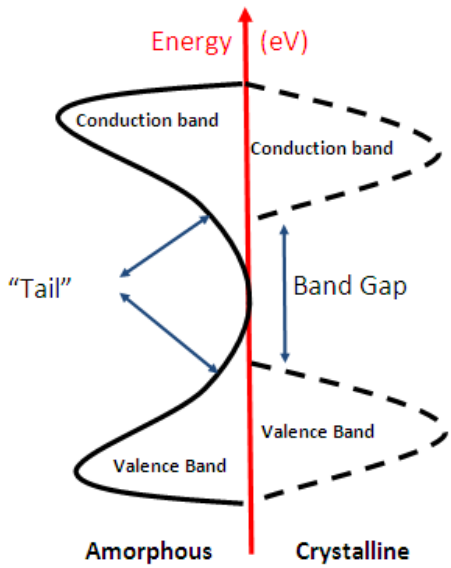

Figure 5. "Tail" extension into band gap region band.

This tail is originated from the weakened/distorted bonds of an amorphous material, and from the presence of deep defects located in the middle of the gap formed by dangling bonds which have a much lower mobility than those bonds outside this region causing a pseudo-gap of mobility [57]. Grein and John [58] observed that for a class of amorphous and disordered semiconductors the optical gap decreases and the absorption tail broadens into the gap region with the increased of structural disorder. Thereby it was conducted a band gap study of the film deposited at 400ºC (best absorpance) to compare the Mo-AlN_xO_y band gap with AlNO, and to observe a possible influence of the molybdenum insertion and amorphous structure in the band gap of the film.

The band gap of AlN, Al_2O_3 and AlN_xO_y are 6.2 eV; 8,0 ~10,0 eV and 6.0 eV, respectively [49]. However, Mo-AlN_xO_y film deposited at 400°C showed a 4.13 eV band gap, **Figure 6** shows the curve of Tauc $(\alpha hu)^2$ x (E). This means that the Mo-AlN_xO_y film has a UV cut-off of approximately 300 nm, as can be seen in **Figure 7**. This result is higher than AlN_xO_y UV cut-off (200 nm) [49], suggesting that the Mo-AlN_xO_y absorbs energy in a region larger than AlN_xO_y.

Besides the amorphous structure, another factor that can reduce the band gap is the molybdenum insertion that produces defects in the structure of the material that may significantly alter its optical performance [59]. According to the theory of bands, these materials have an empty conduction band, whereas the valence band is completely full of electrons. As the band gap of AlN_xO_y is relatively high (6.0 eV), the photons that reach the material are not sufficiently energetic to excite an electron from the

e-ISSN:2321-6212
p-ISSN:2347-2278

valence band to the conduction band. With the inclusion of impurities, called "absorption center", the band gap can be reduced by creating new energy levels [49]. Furthermore, it is worth noting that the optical properties of cermets are strongly influenced by the effect of plasmon resonance that is assigned as the collective oscillations of free electrons of the conduction band of a metal which are embedded in a dielectric matrix. Therewith, the optical properties and energy absorption of the cermet may be adjusted by controlling the size, shape, concentration and distribution of the metal particles in the matrix [60-62]. This can be confirmed by **Figure 6**, wherein the higher absorption at 300 nm corresponds to the film band gap (4.13 eV ≈ 300 nm), or the cut-off of the film, i.e., from this point the reflectance goes up again (**Figure 7**).

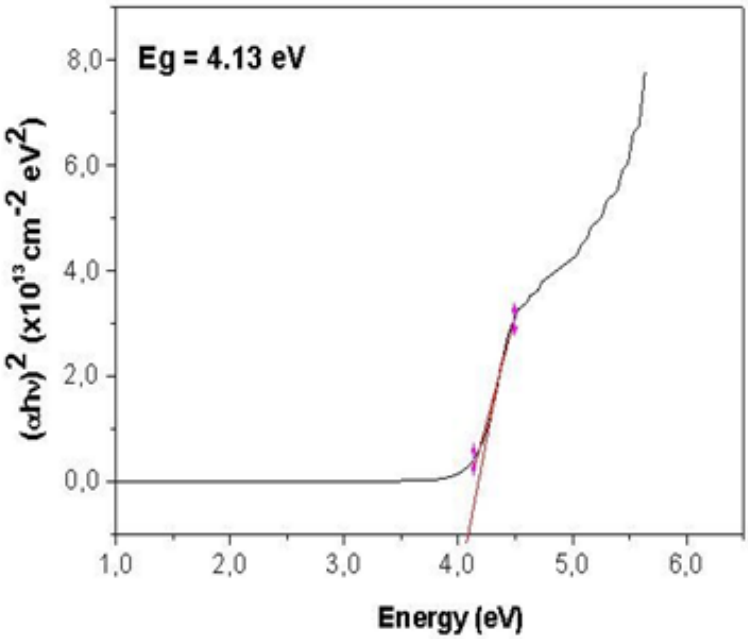

Figure 6. Optical band gap energy of the Mo-AlxNy deposited at 400ºC.

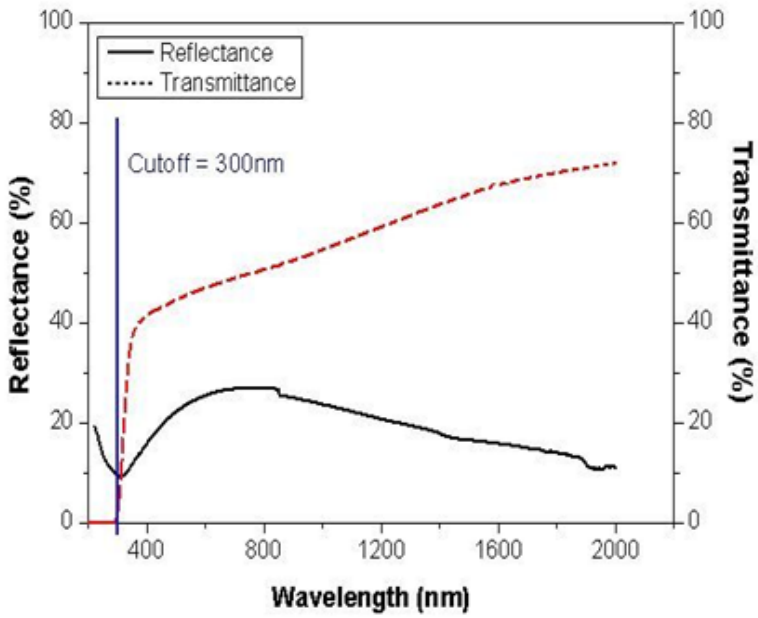

Figure 7. Reflectance and Transmittance of the as-deposited film as a function of the photon wavelength.

The morphological disorder of a film can also be related with the vacancies of the material. In semiconductors such as TiO_2 and Al_2O_3, oxygen vacancies contribute to the absorption in the visible light region, and the nitrogen doping contributes to the oxygen vacancies formation [63]. These oxygen vacancies are able to capture not only holes, but also electrons and to operate as an electron trap in the last case [64]. It is noteworthy that after annealing at high temperature, substitutional nitrogen species in parallel with oxygen vacancies could be favored [63]. The N_2 substitutional insertion increases the photons absorption in the visible region, improving photocatalytic activity of semiconductor material, decreasing the band gap of the material [65]. The effectiveness of the insertion of substitution nitrogen happens because N2p states contribute to decrease the band gap of the material by mix-

e-ISSN:2321-6212
p-ISSN:2347-2278

ing with O2p states and introducing some N2p levels above the valence band O2p [65-67].

CONCLUSION

The deposition of Mo-AlN_xO_y films using a metallic molybdenum tape produced films with homogeneous distribution of Mo. XRD results suggest AlN crystallites embedded in an amorphous matrix of Al_2O_3 located in the bulk of the film. It has also been observed an increase of oxygen concentration with deposition temperature possibly due to the Gibbs free energy. The absorptance increase and band gap reduction was due to the amorphous structure, and molybdenum insertion in the film. The improvement in absorptance occurred in the visible and IR (NIR) regions.

ACKNOWLEDGEMENTS

The author thanks Technological Institute of Aeronautics (ITA); Institute for Advanced Studies (IEav); National Institute for Space Research, Institute of Physics (USP) for the for providing the analysis equipment; National Counsel of Technological and Scientific Development CNPq and São Paulo Research Foundation (FAPESP) for the financial support.

References

1. Brien V and Pigeat P. Correlation between the oxygen content and the morphology of AlN films grown by r.f. magnetron sputtering. J Cryst Growth 2008; 310: 3890-3895.
2. Borges J, et al. AlNxOy thin films deposited by DC reactive magnetron sputtering. Appl Surf Sci 2010; 257: 1478-1483.
3. Chappé JM, et al. Analysis of multifunctional titanium oxycarbide films as a function of oxygen addition. Surf Coat Technol 2012; 206: 2525-2534.
4. Poyai A, et al. High-dielectric constant AlON prepared by RF gas-timing sputtering for high capacitance density. Mater Sci Semicond Process 2008; 11: 319-323.
5. García-Méndez M, et al. Characterization of ALN thin films deposited by DC reactive magnetron sputtering. Revista Mexicana de Física 2008; 54: 271-278.
6. Cheng J, et al. Microwave synthesis of aluminum oxynitride (ALON). J Mater Sci Lett 1999; 18: 1989-1990.
7. Henry BM, et al. A microstructural study of transparent metal oxide gas barrier films. Thin Solid Films 1999; 355-356: 500-505.
8. Erlat AG, et al. Characterisation of aluminium oxynitride gas barrier films. Thin Solid Films 2001; 388: 78-86.
9. Bovard BG. Ion-assisted processing of optical coatings. Thin Solid Films 1991; 206: 224-229.
10. Trinkler L, et al. Use of aluminum nitride for UV radiation dosimetry. Nucl Instrum Meth A 2007; 580: 354-357.
11. Borges J, et al. Electrical properties of AlNxOy thin films prepared by reactive magnetron sputtering. Thin Solid Films 2012; 520: 6709-6717.
12. Engelmark F. AlN and High-k Thin Films for IC and Electroacoustic Applications. Uppsala University. Doctor of Philosophy in Solid State Electronics 78, Sweden 2002.
13. Jakkaraju R, et al. Integrated approaches to electrode and AlN depositions for bulk acoustic wave (BAW) devices. Microelectron Eng 2003; 70: 566-570.
14. García-Gancedo L, et al. AlN-based BAW resonators with CNT electrodes for gravimetric biosensing. Sensor Actuat B-Chem 2011; 160: 1386-1393.
15. Loebl HP, et al. Piezoelectric thin AlN films for bulk acoustic wave (BAW) resonators. Mater Chem Phys 2003; 79: 143-146.
16. Dimitrova V, et al. Aluminium nitride thin films deposited by DC reactive magnetron sputtering. Vacuum 1998; 51: 161-164.
17. Zhang L, et al. Annealing of Al2O3 thin films prepared by atomic layer deposition. J Phys D: Appl Phys 2007; 40: 3707.
18. Hsieh CI, et al. Structural properties of Al2O3 dielectrics grown on TiN metal substrates by atomic layer deposition. Appl Surf Sci 2009; 255: 3769-3772.
19. Chryssou CE and Pitt CW. Al2O3 thin films by plasma-enhanced chemical vapour deposition using trimethyl-amine alane (TMAA) as the Al precursor. Appl Phys A: Mater Sci Process 1997; 65: 469-475.
20. Liao CC, et al. Electrical characterization of Al2O3 on Si from thermally oxidized AlAs and Al. J Crystal Growth 1999; 201-202: 652-655.
21. Wilk GD, et al. High-kappa gate dielectrics: Current status and materials properties considerations. J Appl Phys 2001; 89:

5243-5275.

22. Copel M, et al. Robustness of ultrathin aluminum oxide dielectrics on Si(001). Appl Phys Lett 2001; 78: 2670-2672.
23. Seok AK, et al. Preparation of Al2O3 thin films by atomic layer deposition using dimethylaluminum isopropoxide and water and their reaction mechanisms. Bull Korean Chem Soc 2003; 24: 1659-1663.
24. Lee S and Jeon H. Characteristics of an Al2O3 Thin Film Deposited by a Plasma Enhanced Atomic Layer Deposition Method Using N2O Plasma. Electron Mater Lett 2007; 3: 17-21.
25. Lin C, et al. Electrical properties of Al2O3 gate dielectrics. Microelectron Eng 2003; 66: 830-834.
26. Li Y, et al. Magnetron sputtered nc-Al/alpha-Al2O3 nanocomposite thin films for nonvolatile memory application. J Nanosci Nanotechnol 2009; 9: 4116-4120.
27. Yan Z, et al. Influence of Mo addition on dielectric properties of AlN ceramic matrix composites. J Phys: Conf Ser 2009; 152: 012063.
28. Braga TS, et al. Molibdenium concentration effect in absorptance cermet Mo-AlN composites deposited by magnetron sputtering. Proc IV Brazilian Congress of Solar Energy 2012.
29. Barshilia HC, et al. Structure and optical properties of Ag-Al2O3 nanocermet solar selective coatings prepared using unbalanced magnetron sputtering. Solar Energy Mater Solar Cells 2011; 95: 1707-1715.
30. Wang H, et al. Preparation and characterization of high-toughness ZrB2/Mo composites by hot-pressing process. Int J Refractory Metals Hard Mater 2009; 27: 1024-1026.
31. Kar JP, et al. Influence of rapid thermal annealing on morphological and electrical properties of RF sputtered AlN films. Mater Sci Semicond Process 2005; 8: 646-651.
32. Wäckelgård E and Hultmark G. Industrially sputtered solar absorber surface. Solar Energy Mater Solar Cells 1998; 54: 165-170.
33. Lindgren T, et al. Photoelectrochemical and Optical Properties of Nitrogen Doped Titanium Dioxide Films Prepared by Reactive DC Magnetron Sputtering. J Phys Chem B 2003; 107: 5709-5716.
34. Singh AV, et al. Structural and optical properties of RF magnetron sputtered aluminum nitride films without external substrate heating. Appl Surf Sci 2011; 257: 9568-9573.
35. Cho S, et al. Effect of nitrogen flow ratio on the structural and optical properties of aluminum nitride thin films. J Crystal Growth 2011; 326: 179-182.
36. Dhunna R, et al. Structural and optical properties of AlN/Si system. Mater Sci Semicond Process 2008; 11: 126-130.
37. Totten GE. Handbook of Aluminum: Alloy Production and Materials Manufacturing, Taylor & Francis, New York 2003.
38. Jacobson N. Annual Index for Volume. J Chem Educ 2001; 78: 1713.
39. Mohamed SH, et al. Influence of nitrogen content on properties of direct current sputtered TiOxNy films. Physica Status Solidi (a) 2004; 201: 90-102.
40. Fu R, et al. Morphologies and growth mechanisms of aluminum nitride whiskers synthesized by carbothermal reduction. Mater Sci Eng: A 1999; 266: 44-51.
41. Wu C, et al. Facile solvent-free synthesis of pure-phased AlN nanowhiskers at a low temperature. J Solid State Chem 2004; 177: 3522-3528.
42. Zabinski JS, et al. Stoichiometry and characterization of aluminum oxynitride thin films grown by ion-beam-assisted pulsed laser deposition. Thin Solid Films 2008; 516: 6215-6219.
43. Sczancoski JC. Propriedades mecânicas e tribológicas de Al submetido a nitrocementação por implantação iônica ponta grossa, universidade estadual de ponta grossa, Ponta Grossa 2005.
44. Cullity BD. Elements of X-ray diffraction, Addison-Wesley Publishing Company, Massachusetts 2005.
45. Anders OR. Monteiro, In: L.B.N. Laboratory (Ed.), University of California, Berkeley 2003.
46. Anders AA. Structure zone diagram including plasma-based deposition and ion etching. Thin Solid Films 2010; 518: 4087-4090.
47. Thornton JA. Influence of apparatus geometry and deposition conditions on the structure and topography of thick sputtered coatings. J Vacuum Sci Technol 1974; 11: 666-670.

e-ISSN:2321-6212
p-ISSN:2347-2278

48. Chen Y, et al. Effects of mean free path on the preferentially orientated growth of AlN thin films. J Crystal Growth 2005; 283: 315-319.

49. Ashuach Y. The Influence of Sintering Additives on the Microstructure and Properties of AlON. Faculty of Materials Engineering, Tevet 2003.

50. Huajun S, et al. Influences of Substrate Temperature on Structure, Electrical and Optical Properties of Magnetron Sputtering Ge 2Sb 2Te 5Films. Rare Metal Mater Eng 2010; 39: 377-381.

51. Tian A, et al. Effect of deposition temperature on orientation and electrical properties of (K0. 5Na0. 5) NbO3 thin films by pulsed laser deposition. Appl surf sci 2012; 258: 2674-2678.

52. Dreer S, et al. Statistical evaluation of refractive index, growth rate, hardness and Young's modulus of aluminium oxynitride films. Thin Solid Films 1999; 354: 43-49.

53. Zywitzki O and Hoetzsch G. Influence of coating parameters on the structure and properties of Al2O3 layers reactively deposited by means of pulsed magnetron sputtering. Surf Coat Technol 1996; 86–87.

54. Kennedy CE. In: N.R.E. Laboratory, Colorado, 2002, p. 58.

55. Ilican S, et al. Determination of the thickness and optical constants of transparent indium-doped ZnO thin films by the envelope method. Mater Sci-Poland 2007; 25: 709-718.

56. O'Leary SK, et al. Disorder and optical absorption in amorphous silicon and amorphous germanium. J Non-Cryst Solids 1997; 210: 249-253.

57. Mulato M. in: Physics Department Unicamp, Campinas 1998; 103.

58. Grein CH and John S. Temperature dependence of the Urbach optical absorption edge: A theory of multiple phonon absorption and emission sidebands. Phys Rev B 1989; 39: 1140-1151.

59. Kazan M, et al. Oxygen behavior in aluminum nitride. J Appl Phys 2005; 98: 103529.

60. Selvakumar N and Barshilia HC. Review of physical vapor deposited (PVD) spectrally selective coatings for mid- and high-temperature solar thermal applications. Solar Energy Mater Solar Cells 2012; 98: 1-23.

61. Niklasson GA and Granqvist CG. Optical properties and solar selectivity of coevaporated Co-Al_2O_3 composite films. J Appl Phys 1984, 55: 3382-3410.

62. Pereira MK. In: Instituto de Física, Universidade Federal do Rio Grande do Sul, Porto Alegre 2009.

63. Fujishima A, et al. TiO2 photocatalysis and related surface phenomena. Surf Sci Rep 2008; 63: 515-582.

64. Perevalov TV, et al. Oxygen deficiency defects in amorphous Al2O3. J Appl Phys 2010; 108: 13501.

65. Asahi R and Morikawa T, et al. Visible-Light Photocatalysis in Nitrogen-Doped Titanium Oxides. Sci 2001; 293: 269-271.

66. Yang K, et al. Study of the nitrogen concentration influence on N-doped TiO2 anatase from first-principles calculations. J Phys Chem C 2007; 111: 12086-12090.

67. Khan AA and Labbe JC. Aluminium nitride-molybdenum ceramic matrix composites. Influence of molybdenum addition on electrical, mechanical and thermal properties. J Eur Ceram Soc 1997; 17: 1885-1890.